J. Plasma Physics (1998), *vol.* 59, *part* 2, *pp.* 259–276. Printed in the United Kingdom
© 1998 Cambridge University Press

Stationary operating density profiles in a crossed-field amplifier

D. J. KAUP[1] and GARY E. THOMAS[2]

[1]Institute for Nonlinear Studies and Departments of Physics and Mathematics, Clarkson University, Potsdam, New York 13699-5815, USA

[2]Communications & Power Industries, 150 Sohier Road, Beverly, Massachusetts 01915, USA

(Received 6 January 1997)

We demonstrate with numerical WKB solutions that stationary density profiles can exist in a crossed-field amplifier. These are density profiles that can exist in equilibrium with a high-frequency (RF) wave propagating in the slow-wave structure. These density profiles are very different from the usual Brillouin profiles. They have a finite and negative density gradient, and extend from the cathode to the anode. They carry a DC current proportional to the RF power in the slow-wave structure. The source of the DC current is a wave–particle resonance that occurs toward the top of the sheath. This resonance drives any Brillouin electron flow unstable. The electrons then redistribute themselves into a new flow – one that can be stationary in the presence of the wave–particle resonance. The new flow has a spoke-like structure, where the spokes carry the current to the anode. Various plots are given, including the DC voltage operating range, DC current flow, phase shifts, and density profiles of the total electron distribution, for various ambient magnetic fields and DC voltages. Numerical values agree reasonably well with the modelled experimental device.

1. Introduction

One of the major problems in the theory of crossed-field devices is to devise methods for determining the operating parameters of an operating device. From numerical simulation with PIC codes, one can obtain estimates of these values (Palevski *et al.* 1981; Dombrowski 1988; Riyopoulos 1993), but at a very high cost in computational time. Guiding-centre theory has been used (Davidson 1984; Riyopoulos 1996 and references therein) to develop a nonlinear model in which there is a separation of particle motion into hub motion and spoke motion, as is seen in the numerical simulations. However, this requires a patching of the motion across the hub and the spokes, and also such a theory naturally will require auxiliary parameters, which must be determined. Furthermore, such a model, being based on observations of numerical simulations, tends to lie relatively removed from the basic cold-fluid equations.

In this paper, we report on our results of using a different approach, whereby we decompose the cold-fluid equations into Fourier components, and study the asymptotic solutions of each of the two dominate Fourier components. The purpose of this

https://doi.org/10.1017/S0022377897006363 Published online by Cambridge University Press

study is to determine how well one can describe device characteristics with the cold-fluid equations, and also to use these then as a basis for future studies of the noise characteristics of such devices. Here we demonstrate that by simply inputting the characteristic parameters for a given crossed-field device (such as dimensions, dispersion curve for the slow-wave structure, operating frequency, ambient magnetic field), we can predict, reasonably well, the actual operating voltage range of the device versus the ambient magnetic field, as well as the net phase shift that occurs inside the device and also the operating current density. Furthermore, when we reconstruct the total density from the two main Fourier components, the resulting density profiles are very similar to those seen in numerical simulations. However, our solutions are much smoother, being WKB solutions of the cold-fluid equations and not simulations.

The theory and background of this work has been well detailed in previous works (Kaup and Thomas 1996, 1997). To summarize those results, the so-called magnetron instability (Buneman *et al.* 1966; Antonsen *et al.* 1985) seems to have little to do with the actual operation of crossed-field devices (Jablonski 1992). The instability is indeed there (Buneman 1966), and we do observe effects due to it. However, its importance to the operation of a crossed-field device is considerably less than the wave–particle interaction (diocotron). Furthermore, we have been able to show that the classical Brillouin flow (Brillouin 1945) in such devices is nonlinearly unstable (Kaup and Thomas 1996) to the presence of high-frequency (RF) waves propagating in the slow-wave structures that these devices contain. The instability initializes as a linear wave–particle instability in a Rayleigh-like equation with a shear flow. Once this linear instability initializes, it will trigger the nonlinear instability, which is a consequence of second-order (quasilinear) theory (Davidson and Tang 1985; Davidson 1985; Kaup and Thomas 1989). The growth rate of this nonlinear instability is directly proportional to the density gradient at the edge of the sheath (Kaup and Thomas 1996), which for a Brillouin flow is very large. The second-order theory then predicts that the electron density will change and evolve. What we find is that it does evolve and it does relax to a new density profile, which is one that will be in equilibrium with the propagating RF wave. This instability of the Brillouin sheath is not surprising since earlier kinetic studies in magnetically insulated diodes (Desjarlais and Sudan 1986, 1987) had revealed that stochastic electron motion occurs as the Brillouin limit is approached. Thus electrons in a Brillouin flow can be easily perturbed, and kicked out of the flow and into new states.

The physics of this instability is quite simple. One starts with a CFA where the ambient magnetic field is present, the input RF signal is present, and the DC voltage is off and at zero. Presumably, there are a few free electrons present, which, by secondary emission, will generate the electron plasma. The input RF signal has a fixed RF frequency ω, and inside the device it also has a characteristic RF wave vector k, which is determined by the dimensions and characteristics of the device and its slow-wave structure. One now turns on the DC voltage. However, it requires hundreds of oscillations before the DC voltage will reach its final value. As this voltage slowly increases, secondary emission is generating free electrons and a sheath of electrons undergoing a classical Brillouin flow is created. At first, this sheath is so thin that no wave–particle interaction with the RF wave in the slow-wave structure can occur. While the DC voltage is rising and the device is being filled with plasma, the RF wave vector shifts toward smaller values, since the plasma

https://doi.org/10.1017/S0022377897006363 Published online by Cambridge University Press

appears as a conductor to the RF wave. Eventually the sheath becomes sufficiently thick for wave–particle interactions to occur. When this happens, the electrons at the top of the sheath will have a drift velocity v_d equal to the phase velocity ω/k of the RF wave. Exactly when this occurs will depend on the value of k, which does shift as the sheath grows. As the wave–particle interaction turns on, depending on the relative phase of the now seemingly stationary (to the electrons) RF electric field, the initially uniformly distributed electrons can now be bunched and/or accelerated. Some of these electrons will be accelerated, cascading toward the anode. Others will be decelerated, possibly spiraling back into the sheath. In any case, a pattern will develop quite rapidly, with a basic spatial, moving periodicity of $2\pi/k$, propagating on an altered background. The problem is therefore to determine this pattern and the altered average background, on which this pattern will propagate.

The relatively slow rise time of the applied DC voltage allows us to approximate this process adiabatically. Owing to the rapid nonlinear growth rate of the instability, at any instant, we can consider the applied DC voltage to be a constant, as far as the nonlinear instability is concerned. Thus, at each value of the applied DC voltage, we can expect the electron density profile to have responded to the demands of the nonlinear instability, achieving a stationary state (Kaup and Thomas 1989) for that voltage. These stationary states are, in general, quite different from the classical Brillouin density profiles. In particular, they all have finite, negative density gradients, and they all extend from the cathode to the anode, with a nonzero value of the density at the anode (Kaup and Thomas 1989). Furthermore, each state has a nonzero DC current flow where the DC current is proportional to the RF input power. Thus the device acts as an amplifier, delivering power to the RF wave, proportional to the local RF energy density.

Here we shall take the major equations from our previous studies and apply them to a specific tube, calculating the operating density profiles, the operating voltage range, the phase shift per section and the operating current density. The essential equations will be described and discussed in Sec. 2 and the numerical results will be presented in Sec. 3. In Sec. 4, we shall discuss the results of – and defects of – the current model, indicating what improvements could be made in the future.

2. Basic equations

The geometry and configuration that we shall be using are shown in Fig. 1, which is a diagram of a 'planar magnetron'. A planar geometry is preferred for analytical treatment because of its simplicity. Although actual devices are usually cylindrical, the essential physics are contained in the planar model. At the bottom is the cathode, which is an electron-emitting material. It is located in the (x, z) plane at $y = 0$. We take the ambient magnetic field to be along the negative z axis, so that the electron drift velocity will be in the positive x direction. The electron cyclotron frequency is $\Omega = eB_0/mc$, where B_0 is the ambient magnetic field. Next to the cathode is the electron sheath which extends out for some distance from the cathode. The anode is located at a distance l above the cathode. On the anode is a slow-wave structure which is simply a waveguide, along which the RF wave will propagate. This slow-wave structure is there (i) to slow down the electromagnetic RF wave, which is moving near the speed of light inside the anode structure and (ii) to select the effective RF (electrostatic) wave vector k that the plasma will see and will respond to.

https://doi.org/10.1017/S0022377897006363 Published online by Cambridge University Press

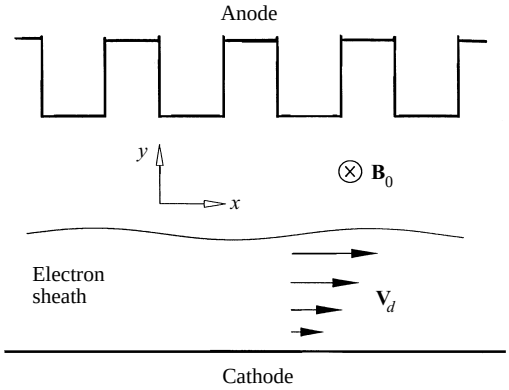


Figure 1. The geometry and configuration of a planar magnetron or CFA. The magnetic field is directed into the paper and the electron drift velocity is to the right. The z axis is perpendicular to the paper, the x axis is parallel to the cathode surface and the y axis is perpendicular to the cathode.

The basic cold-fluid equations describing this physical system are

$$\partial_t n + \nabla \cdot (\mathbf{v}n) = 0, \tag{1}$$

$$\partial_t \mathbf{v} + (\mathbf{v} \cdot \nabla)\mathbf{v} - \nabla\phi + \mathbf{v} \times \mathbf{\Omega} = 0, \tag{2}$$

$$\nabla^2 \phi = n. \tag{3}$$

In these equations, the fluid velocity vector is in the (x, y) plane and all quantities are taken to be independent of the z coordinate. We have also simplified the notation by taking n to be the square of the electron plasma frequency ($4\pi e^2 \rho/m$, where e and m are the electronic charge and mass respectively and ρ is the electron number density) and ϕ to be e/m times the electrostatic potential. We shall use this notation in the remainder of the paper.

These equations (1)–(3) are then expanded in Fourier components of $e^{i(kx-\omega t)}$ (Kaup and Thomas 1989). On the fast time scale, the DC Fourier component of this expansion gives the 'background solution', which satisfies

$$\mathbf{v} = v_0(y)\hat{\mathbf{x}}, \tag{4}$$

$$v_0(y) = \partial_y \phi_0(y)/\mathbf{\Omega}, \tag{5}$$

where ϕ_0 is obtained from Poisson's equation

$$\partial_y^2 \phi_0 = n_0, \qquad \phi_0(0) = 0 = \partial_y \phi_0(0) \tag{6}$$

and where we have taken the background potential ϕ_0 to be zero at the cathode ($y = 0$) and have imposed the space-charge-limited current condition $\partial_y \phi_0(0) = 0$. Thus, from (6), the solution for $\phi_0(y)$ is determined once $n_0(y)$ is given. On this fast time scale, the background electron density profile, $n_0(y)$, is arbitrary, except that it does have to satisfy one integral condition, namely that the potential at the anode, $\phi_0(y = l)$, must equal the applied cathode–anode DC voltage V_0. Also, if the background electron density profile is to be linearly stable then it is necessary for the density profile to always have a nonpositive density gradient (Davidson 1985).

Next we consider the fast time scale of the fundamental Fourier components of these equations in the presence of the above background. These can be reduced to

https://doi.org/10.1017/S0022377897006363 Published online by Cambridge University Press

(Buneman *et al.* 1966; Kaup and Thomas 1989)

$$\partial_y p = Au, \tag{7}$$

$$\partial_y u = Bp, \tag{8}$$

where

$$A = \Omega^2 - \omega_e^2, \tag{9}$$

$$B = \frac{k^2}{A} - \frac{k\partial_y n_0}{\Omega\omega_e A} - \frac{2k^2 n_0 \Delta^2}{\Omega^2 A^2}, \tag{10}$$

$$u = -ikv_{1x}, \tag{11}$$

$$p = Av_{1y}, \tag{12}$$

$$\omega_e = \omega - kv_0, \tag{13}$$

$$\Delta^2 = \Omega^2 - n_0. \tag{14}$$

Here ω_e is the frequency of the RF wave as seen by the electron moving at the background drift velocity $v_0(y)$, and Δ is the local orbital oscillating frequency for individual particle orbits (Prasad *et al.* 1987; Kaup and Thomas 1992), which would vanish for a Brillouin flow. In (11) and (12), v_{1x} and v_{1y} are the x and y components of the perturbed velocity fields. The perturbed electrostatic potential ϕ_1, its gradient $\partial_y\phi_1$ and the perturbed electron density n_1 are obtained from p and u as follows (Kaup and Thomas 1989):

$$n_1 = ip\left(\frac{2kn_0^2}{\Omega A^2} - \frac{\partial_y n_0}{A\omega_e}\right), \tag{15}$$

$$\phi_1 = \frac{ip\Delta^2}{Ak\Omega} - \frac{iu\omega_e}{k^2}, \tag{16}$$

$$\partial_y\phi_1 = \frac{i\Omega}{k}u - \frac{i\omega_e}{A}p. \tag{17}$$

The boundary conditions on (7) and (8) follow from the boundary conditions on ϕ_1. At the cathode, which is grounded, the perturbed potential must vanish. Thus $\phi_1(y = 0) = 0$. Then by (16), one has the ratio of u to p at $y = 0$ determined. This determines the solution up to an overall magnitude. One must still match this solution from the cathode–anode region to the solution inside the slow-wave structure. In general, this will only occur for selected values of k and γ (= Im(ω)), which give the possible eigenmodes of these equations. For any eigenmode, its magnitude can finally be normalized to some fixed value of E_{xa}, which is the value of E_x at the vane tips of the slow-wave structure.

Next we return to the DC Fourier component and consider the next-order slower time scale, which is second order in the amplitude. Once we have a small RF signal oscillating in the device as described above, after many oscillations, owing to the nonlinearities in (1)–(3), shifts will start to occur in the background quantities. An analysis of all such shifts was given in Kaup and Thomas (1989), and the results are effectively the same as in the quasilinear theory of Davidson (1985). The main result is that the background potential (and the background density profile) will evolve according to

$$\partial_\tau\partial_y\phi_0 - \Delta^2 C_2 = D\partial_y n_0, \tag{18}$$

https://doi.org/10.1017/S0022377897006363 Published online by Cambridge University Press

where C_2 is a constant of integration, τ is a slow time variable and

$$D = \sum_k \frac{2\gamma p^* p}{\omega_e^* \omega_e A^* A} e^{2\gamma t}, \tag{19}$$

which is the quasilinear diffusion coefficient. In (19), the sum is over all modes, and γ is the growth rate, which is the imaginary part of the RF frequency, ω. Furthermore, this is the asymptotic value of D, in the limit that γt is sufficiently large, such that one can ignore the decaying part of the solution. The quasilinear diffusion equation is obtained upon differentiating (18) once. Then, from (6) and (14), one finds

$$\partial_\tau n_0 + C_2 \partial_y n_0 = \partial_y (D \partial_y n_0). \tag{20}$$

We now use the adiabatic approximation and impose the condition that n_0 is to be an equilibrium, or stationary, density profile, which means that the first term in (20) is taken to vanish. Furthermore, we shall also impose the condition that any electron touching the anode will immediately be absorbed by it. Consequently, the density profile will vanish at the anode. Then, upon integrating (20), this gives (Kaup and Thomas 1996)

$$n_0 = \Omega^2 \left[1 - \exp\left(-C_2 \int_y^l \frac{dy}{D} \right) \right], \tag{21}$$

which defines the steady-state equilibrium density profile in terms of the quasilinear diffusion coefficient and the constant C_2. Given D and C_2, this density profile then determines the DC electrostatic potential Φ_0, and therefore the applied DC voltage V_0. However, there are no conditions on C_2, and by varying C_2 one can therefore change V_0. Conversely, fixing V_0 will determine a particular value of C_2. For the stationary states, the significance of C_2 is that it gives the asymptotic DC current density. One may show that the second-order DC current density is given by (Kaup and Thomas 1996)

$$J_{2y} = C_2 \Omega^2, \tag{22}$$

which is a constant, uniform, vertical particle flux.

Thus we now have a means of determining the background DC density profile in an operating device in the adiabatic limit. One wants those density profiles that are in equilibrium with the RF wave propagating in the slow-wave structure. The eigenmodes of an RF wave propagating on this density profile could have various different eigenmodes, each of which would satisfy (7) and (8). One would include all these various eigenmodes in the evaluation of the diffusion coefficient by (19). Of all these modes, only the unstable ones need be included, since γ is zero for the stable modes. Furthermore, in the asymptotic limit, since the most-unstable mode will dominate, we need to retain only that mode in the sum. Thus we shall take

$$D = \left. \frac{2\gamma p^* p}{\omega_e^* \omega_e A^* A} e^{2\gamma t} \right|_{\text{most unstable}}. \tag{23}$$

Now the problem becomes one of consistency. Can we find a density profile $n_0(y)$ that is stationary and for which the most unstable RF eigenmode (for the given slow-wave structure) generates a diffusion coefficient, which, by (21), regenerates the same $n_0(y)$? It turns out that such profiles do exist and they can be determined numerically. Such will be demonstrated in the next section for a particular CFA.

https://doi.org/10.1017/S0022377897006363 Published online by Cambridge University Press

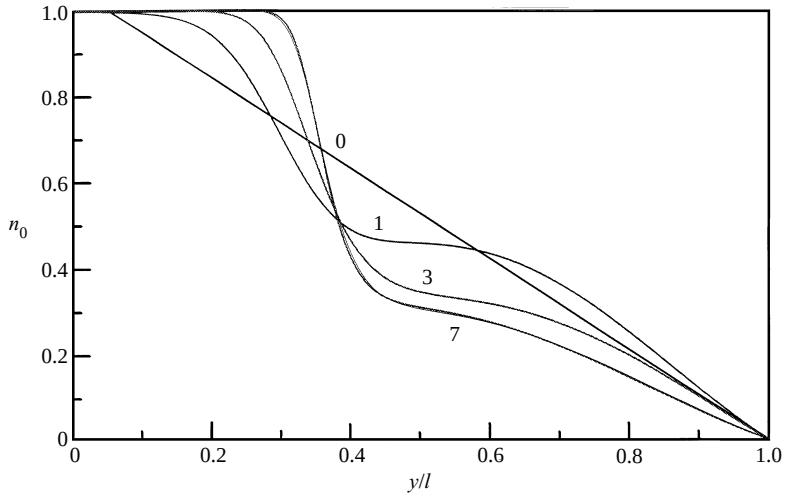


Figure 2. A demonstration of the convergence to a stationary density profile, normalized to the Brillouin value of Ω^2. The DC voltage is 0.70 of the cutoff voltage, l is the anode–cathode spacing, and $\omega_0/\Omega = 0.90$, where ω_0 is the RF frequency used in these calculations. The numbers refer to the iteration number, with zero being the initial ramped density profile. Iteration was continued until k, γ and C_2 changed by no more than 1%. Not all iterations are shown.

3. Numerical solutions

If the stationary density profile is a reasonably stable fixed point of these equations then we should be able to converge to it from almost any reasonable initial density profile. Thus one should be able to choose some reasonable initial guess for a density profile, calculate the RF eigenvalues for k and γ, find the most-unstable mode, and use that mode to evaluate D by (23). Now, in order to construct a new density profile from (21), one needs some value for C_2. This can be determined by choosing values for C_2, evaluating (21), and integrating twice to find the applied DC voltage V_0 for that density profile. Now one varies C_2 until the resulting V_0 is the correct value. Once this is accomplished, one then has a new density profile, which should be closer to the desired stationary profile. One now recalculates the RF fields, recalculates D and C_2, and obtains another density profile. Continuing in this manner, one finds that the procedure does converge to a stationary density profile.

For numerical simplicity, we shall initially choose a broad, ramped density profile to start with, as shown in Fig. 2, the curve labelled '0'. For any density profile $n_0(y)$ and any RF frequency ω, there are usually only one or two unstable eigenmodes of the RF equations, (7) and (8). We shall use the modified WKB approximation described in Kaup and Thomas (1996) for the numerical calculations.

To obtain numerical solutions, it is necessary to chose a model for the slow-wave structure. The slow-wave structure is a waveguide along which an electromagnetic RF wave can propagate. In the absence of a plasma, it has a dispersion relation $\omega_{ct}(k)$ that defines the modes that can propagate along it. In the presence of a plasma, this dispersion relation will be shifted, depending on how the plasma interacts with the fringe field of the RF wave propagating in the structure. Since we are assuming that the plasma never penetrates into the slow-wave structure, we can take the region inside the structure to always be a vacuum region. Therefore,

https://doi.org/10.1017/S0022377897006363 Published online by Cambridge University Press

inside this region, using Maxwell's equations and taking k and ω to be independent variables, one can solve for the electromagnetic fields inside the structure (Slater 1959; Davidson *et al.* 1991; Chan *et al.* 1993), from which one can determine the fields along the tips of the vanes. In particular, at the tips of the vanes, there will be a definite value for the ratio of the averaged x and y components of the RF electric field, for any given k and ω. (The overall magnitude of these fields will be determined by the power level of the RF field in the slow-wave structure.) This is the value that one must match to the RF plasma solution. Note that we can determine this ratio for the slow-wave structure independently of the plasma solution, since the slow-wave structure is a vacuum region and thus this ratio will only be a function of k and ω.

The only experimental data available for this particular slow-wave structure is the cold-test dispersion curve ($\omega_{ct}(k)$). To extend off of the cold-test curve, and to determine the ratio of the components of the averaged RF fields for other k values (at the same RF frequency), we shall use a modified comb model, constructed in the following manner. Define $\rho_{\rm sws}(k,\omega) = -iE_{xa}/E_{ya}$, where E_{xa} and E_{ya} are the x and y components of the RF electric field inside the slow-wave structure, evaluated and averaged at the vane tips. The same quantity for the plasma solution will be $\rho_{\rm plasma} = k\phi_1(l)/\partial_y\phi_1(l)$ which is the scaled inverse of the logarithmic derivative of the RF electrostatic potential for the plasma solution at the vane tips. For a pure comb model (Slater 1959; Davidson *et al.* 1991; Chan *et al.* 1993), we have $\rho_{\rm sws}(k,\omega) = f(k)g(\omega)$, where $f(k)$ is some function of k and $g(\omega) = \omega\tan(s\omega/c)$, with s being the vane depth and c the speed of light. So, let us take

$$\rho_{\rm sws}(k,\omega) = \frac{g(\omega)}{g(\omega_{ct}(k))}\rho_{\rm sws,ct}(k,\omega), \tag{24}$$

where (Slater 1959; Davidson *et al.* 1991; Chan *et al.* 1993)

$$\rho_{\rm sws,ct}(k,\omega) = \frac{\kappa}{k}\tanh(\kappa l) \tag{25}$$

and $\kappa = (k^2 - \omega^2/c^2)^{1/2}$ with the subscripts 'ct' indicating the cold-test values. Then $\rho_{\rm sws}(k,\omega)$ will have the correct cold-test limit and otherwise will behave as a comb model. We shall treat the vane depth s as a free parameter, since if we used the correct value of s, we should have the wrong value for the π mode. Rather, we set s so that the π mode occurs at the correct frequency. The resulting curves for $\rho_{\rm sws}(k,\omega)$ for three different frequencies are shown in Fig. 3.

Let us now return to Fig. 2. Here we demonstrate the convergence of our method for finding stationary density profiles. Curve 0 is the initial density profile. We iterate as described above, calculating the RF fields, finding the eigenmode with the largest growth rate, calculating D from this, using (21) to determine C_2 and the next density profile. As one can see, the profiles are converging to a well-defined, stationary, density profile. (This iteration was stopped at iteration 7, for which the changes in C_2 and in the eigenvalues k and γ had become less than 1%.) We have found this to be a very general feature of these equations. In all cases so far investigated, where there is at least one unstable mode, this method of solution of the stationary density profiles has been convergent.

Let us now look at a series of such profiles as shown in Fig. 4, where V is given in units of the cutoff voltage of the ambient magnetic field. Here we have set $\omega/\Omega = 0.9$ and then varied the DC voltage, looking for possible stationary density

https://doi.org/10.1017/S0022377897006363 Published online by Cambridge University Press

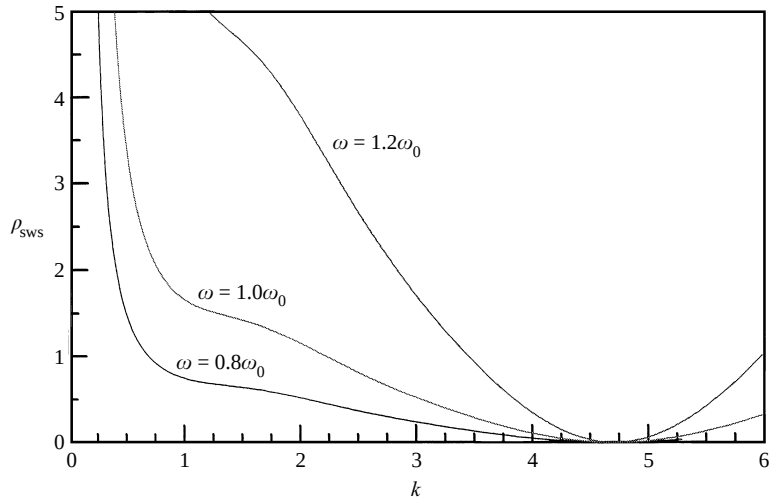


Figure 3. Plots of $\rho_{sws}(k, \omega)$ of the modified comb model that was used in these calculations. ω_0 is the RF frequency used in the calculations and l is the anode-cathode spacing.

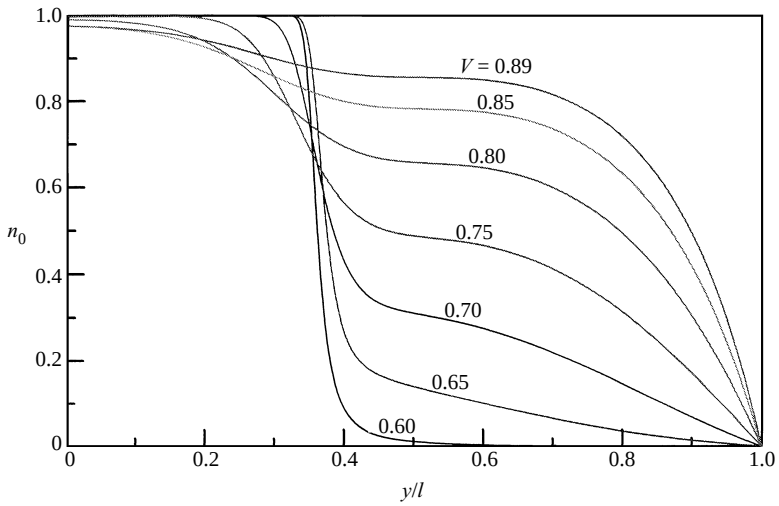


Figure 4. Stationary density profiles obtained for $\omega_0/\Omega = 0.9$, where V is the applied DC voltage, in units of the cutoff voltage for this cyclotron frequency Ω. At $V = 0.60$, the tube is nonconducting and is just below turn-on, which occurs at $V = 0.62$. Note the clear Brillouin structure in this limit. At $V = 0.65$, a distinct ramp structure forms and the tube becomes conducting. At higher voltages, the current increases and the ramp turns into a relatively high-density plateau. At $V = 0.90$ (not shown), this system does not seem to have a stationary density profile.

profiles. No such solutions seem to exist for $V \leqslant 0.60$. For $V \geqslant 0.61$, we definitely have stationary density profiles. In the figure, we show that, just above threshhold, at $V = 0.65$, a small ramp structure forms on the Brillouin flow that contains the conducting electrons. As the DC voltage rises, this ramp deforms into a plateau-like structure, with a higher and higher electron density, and at the same time, the current also increases, owing to the increased number of electrons available in

https://doi.org/10.1017/S0022377897006363 Published online by Cambridge University Press

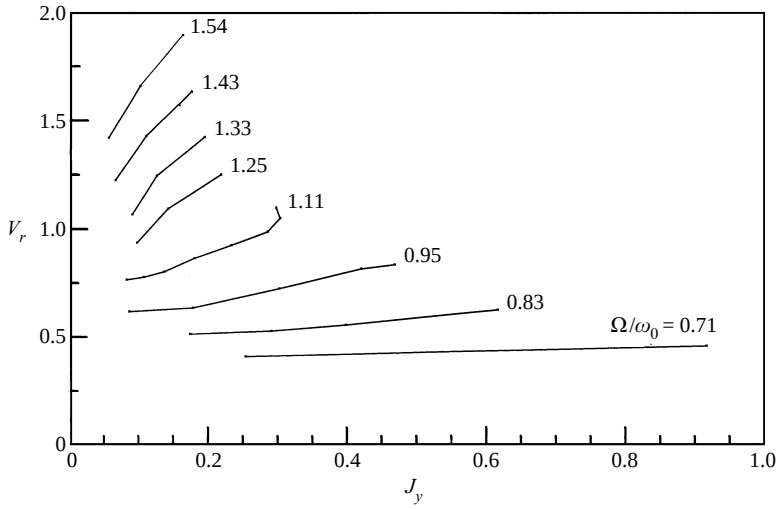


Figure 5. Current density for selected stationary density profiles, for a fixed x component of the RF electric field at the vane tips, as a function of the DC voltage V_r and for various values of the magnetic field. Here V_r is measured in units of the cutoff voltage for the cyclotron frequency Ω equal to the RF frequency ω_0. This figure also outlines the possible DC voltage operating regime as a function of the ambient magnetic field.

the region. Finally, at $V = 0.89$, the stationary density profile has expanded to occupy almost all the vacuum region. For $V = 0.90$, no such stationary density profile seems to exist, in spite of our searching. The conclusion is that the region $0.62 \leqslant V \leqslant 0.89$ is a possible operating regime, and that, outside this region, the tube would not be expected to operate. We shall discuss these points more fully in the last section.

In Fig. 5, we expand the above calculations to include several other values of the magnetic field, keeping the RF frequency fixed. Here we present the asymptotic DC current density, as calculate from (22), taking the x component of the RF electric field to have a common value for all the DC voltages and ambient magnetic fields. While this condition could be questioned, it nevertheless provides us with a means of commonly comparing the DC currents at different DC voltages and ambient magnetic fields. Here V_r is the DC voltage in units of that cutoff voltage where the cyclotron frequency is equal to the RF operating frequency, i.e. $\Omega = \omega_0$. When one takes into consideration the surface area of the experimental device, the DC current densities in this figure are comparable to the experimental values. This point will also be further discussed in the last section. For comparison, the experimental analogue of Fig. 5 is shown in Fig. 6. Note that the DC voltage and cyclotron frequencies are in the same units as in Fig. 5; however, the DC current is in arbitrary units. What one can observe here is that both curves have the same general trends, but with Fig. 5 containing a wider range of values.

Figure 7 is similar to Fig. 5, except that it is for the phase shift per section. Again, these values are in reasonable agreement with the experimental values.

Now, let us go a step further. We have numerical solutions for the background fields (up to second order) as well as for the lowest order of the RF fields. Let us combine these together and see what the total solution would appear to be. In Fig. 8, we have composed such a solution for the $V = 0.65$ solution in Fig. 4, using

https://doi.org/10.1017/S0022377897006363 Published online by Cambridge University Press

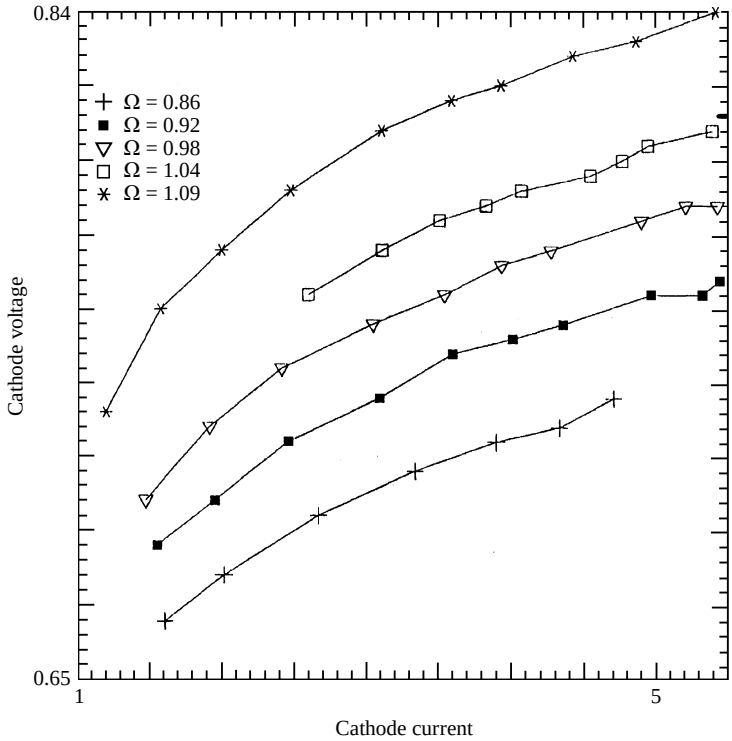


Figure 6. Experimental curves corresponding to Fig. 5. The current is in arbitrary units, but the values of the cyclotron frequency and the DC voltages are in the same units as in Fig. 5. There is a cutoff at the upper range of current, due to a limitation in the current-measuring device used.

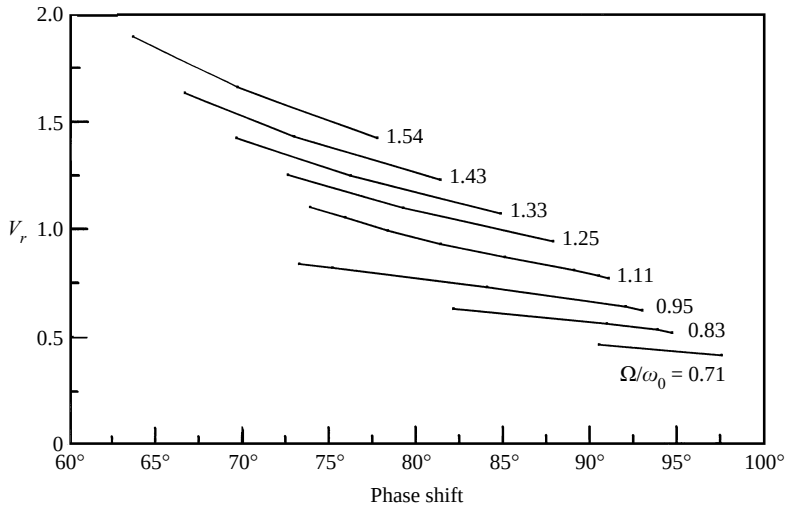


Figure 7. Same as Fig. 5, but for the phase shift per section.

https://doi.org/10.1017/S0022377897006363 Published online by Cambridge University Press

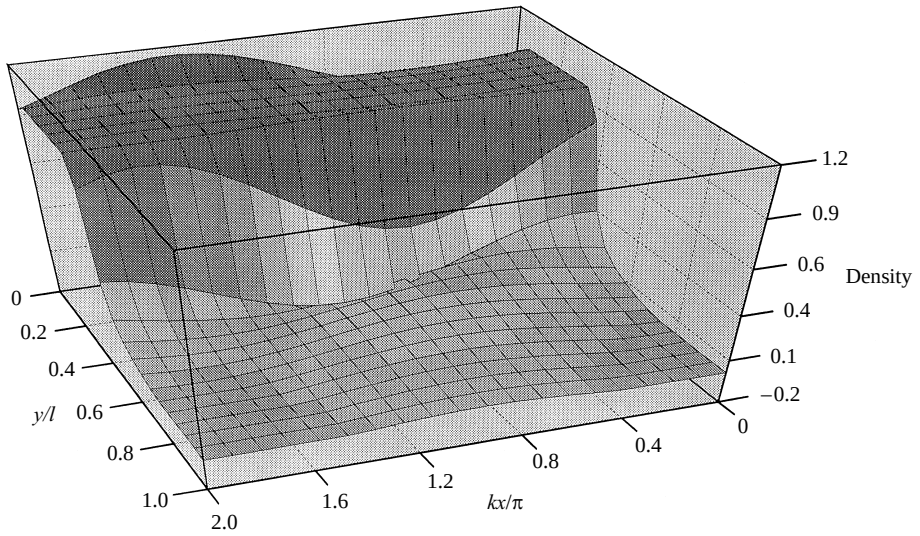


Figure 8. Plot of the asymptotic solution for $n(x, y)$ versus x and y for one period of the propagating RF wave, and for the $V = 0.65$ solution shown in Fig. 4. The x component of the RF electric field at the vane tips is the same as in Fig. 5. Note the structure in the foreground, which is the spoke of charge, reaching the anode and carrying the DC current. The slow oscillation seen near the cathode and deep in the sheath is due to the 'magnetron resonance', where $\omega_e = \Omega$. However since $\omega_0 < \Omega$, the resonance does not occur inside the physical region, and one is only seeing a disturbance due its close proximity in phase space.

the same RF amplitude as in Fig. 5. One notes three distinct features. First, there is the characteristic high-density, Brillouin flow around the cathode. Secondly, in the middle of the foreground, there is a weak 'spoke' of charge reaching up to and touching the anode. (In the region near the anode, certain parts of the solution were negative. We have replaced those negative values by zeros. We shall discuss and justify this approach later.) This is the source of the DC current. Thirdly, one notes that near the cathode, there are relatively large oscillations occurring deep in the sheath where v_0 is very small. These oscillations are due to an almost zero in A, since ω_e is almost equal to Ω in that region (the so-called magnetron resonance) (Antonsen *et al.* 1985). In Fig. 9, we compare the magnitude of n_1 (the Fourier component) with n_0 and plot each as functions of y. Again, one can see the same three features as in Fig. 8, plus one more, namely the very distinct peak in $|n_1|$ at the edge of the Brillouin sheath. This is the value of y at which the wave–particle resonance occurs ($\omega_e = 0$), and this peak shows that a large fraction of the particles at that position are being perturbed.

In drawing Fig. 9, it was necessary for us to normalize the RF amplitude to some value. We chose this normalization factor so that, as is easily seen in Fig. 9, the amplitude of the RF field would be as large as possible, without creating unphysical (negative) density regions. (The total density is $n_0 + \mathrm{Re}[n_1 e^{i(kx-\omega t)}]$, where Re indicates the real part.) Thus, to keep the total density positive for all values of x and t, we must maintain $|n_1| < n_0$. We could easily do this for all regions except near the anode. Here, since the boundary condition on n_0 is $n_0(y = l) = 0$, it is impossible to achieve. However, one must remember that so far we have ignored

https://doi.org/10.1017/S0022377897006363 Published online by Cambridge University Press

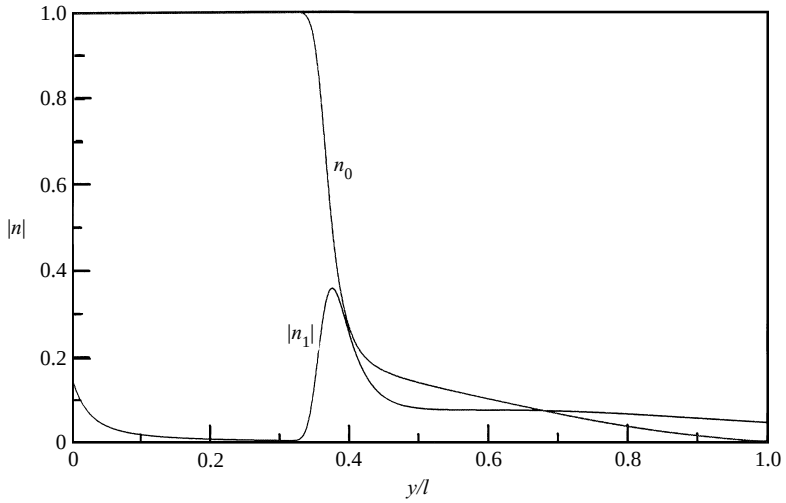


Figure 9. Plot of the magnitude of the RF density $n_1(y)$ in comparison with the background density $n_0(y)$ for the solution in Fig. 8. Note that this is the largest expected value of the RF density, since a larger value would give a negative (unphysical) density in the region of the resonance, near $y = 0.38$. Near the anode, one expects the higher-order harmonics to become significant, which would then maintain a positive density in that region. (See the discussion in Sec. 4.)

all the higher harmonics; terms such as $\mathrm{Re}[n_2^{(2)}(y)e^{2i(kx-\omega t)}]$ in the notation of Kaup and Thomas (1989). These terms can be expected to be important only in the region near the anode. Consequently, if one did evaluate them and include them in the total density, one can expect their phases to be such as to cancel the negative values of the total density. We shall return to this point in the last section. But, for now, we shall therefore allow $|n_1|$ to exceed n_0 near the anode, and when we calculate the total density by using only the two leading terms, we shall replace all negative values with zeros.

In Fig. 10, we show the magnitudes of the Lagrangian displacements for the RF motion of the particles for the $V = 0.65$ solution in Fig. 5. These displacements are related to p and u by (Drazin and Reid 1981)

$$\xi_x = in_0\xi_y - \frac{u}{k\omega_e}, \qquad \xi_y = i\frac{p}{A\omega_e}. \tag{26}$$

As is clear from the figure, at the resonance, there is very large x displacement, with the particles undergoing strongly elliptical oscillations, with the x displacement even larger than the anode–cathode spacing. However, well above the resonance, in the vacuum region, this motion relaxes to a simple circular cyclotron motion.

In Fig. 11, we show the magnitudes of the RF electrical fields for the $V = 0.65$ solution in Fig. 4. As one can see, these fields remain essentially zero inside the sheath, where the particles tend to shield them out.

The $V = 0.65$ solution in Fig. 4 is a solution just above threshhold. Let us now consider another solution – one that is well above threshhold, has a larger DC current, a larger DC voltage, $V = 0.70$, and a larger ambient magnetic field, $\Omega = 1.25\omega_0$. In Fig. 12, we show the comparison of the background density with the

https://doi.org/10.1017/S0022377897006363 Published online by Cambridge University Press

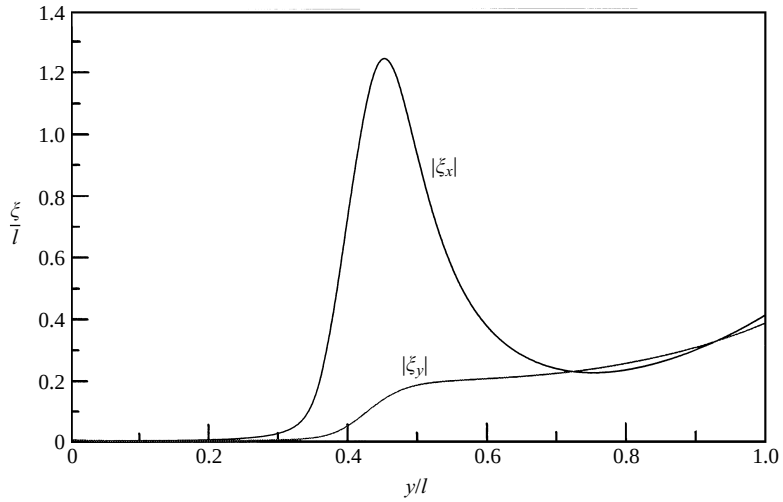


Figure 10. Plot of the magnitudes of the RF Lagrangian displacements for the solution in Fig. 8, as a function of y. Note that at the resonance, ξ_x becomes very large, which results in very large horizontal excursions of the electrons. Above the resonance, the particle motion become a simple circular cyclotron motion.

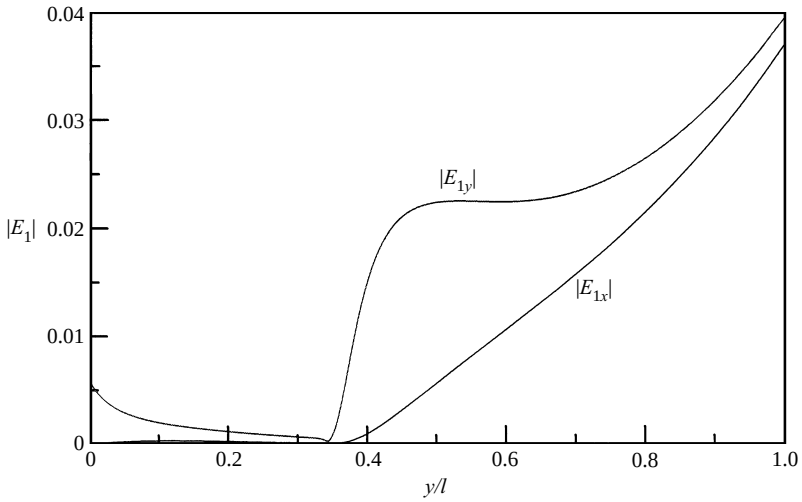


Figure 11. Plot of the magnitudes of the RF electrical fields for the solution in Fig. 8, as functions of y. Note that inside the plasma, the particles tend to shield these fields.

amplitude of the RF density. In this case, we can take the x component of the RF electric field at the anode to be four times that of the previous example. Note that the formation of the plateau region has allowed the RF fields to become larger. This represents a 16-fold increase in the local RF power. The total density as a function of x and y is shown in Fig. 13. This is similar to Fig. 8, except that now one sees a much larger spoke of charge extending up to the anode. Plots of the Lagrangian displacements and the RF electric field (not shown) are similar to those for the $V = 0.65$ case, except that the amplitudes are correspondingly larger.

https://doi.org/10.1017/S0022377897006363 Published online by Cambridge University Press

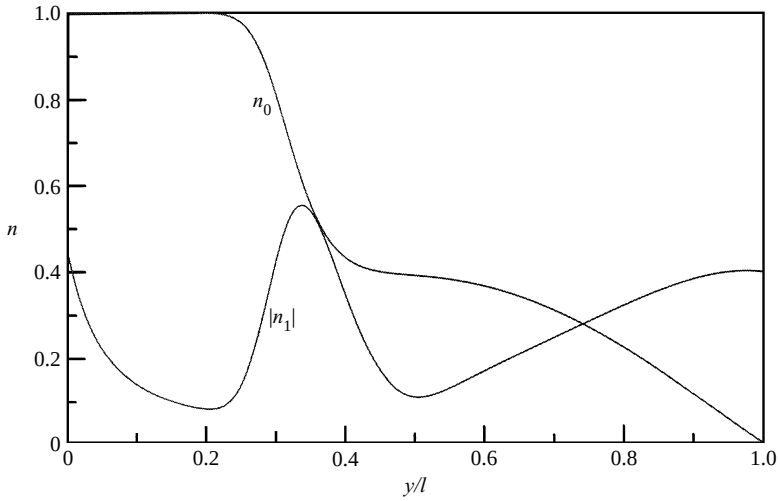


Figure 12. Plot of the magnitude of the RF density $n_1(y)$, in comparison with the background density $n_0(y)$ for a higher-DC-current case; $V = 0.70$ and $\Omega/\omega_0 = 1.25$. Here we can take the RF amplitudes to be four times that in Fig. 5.

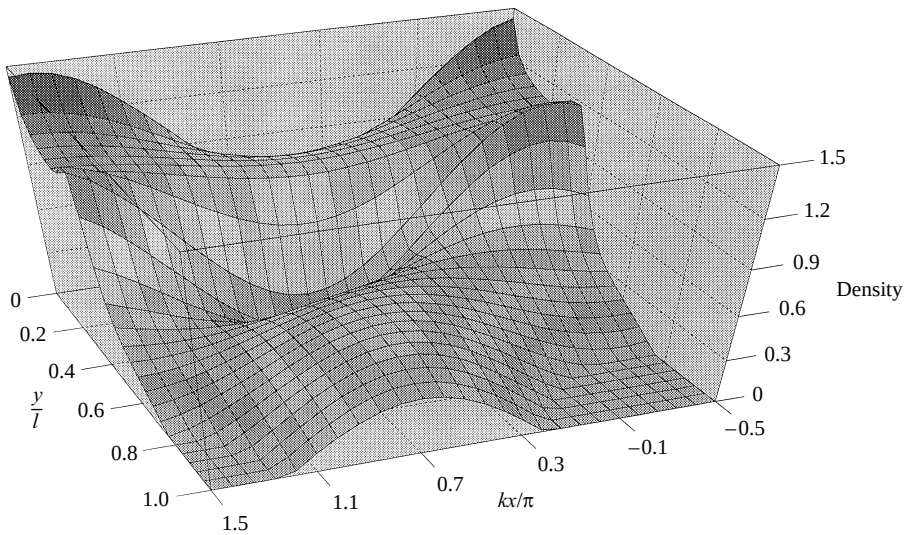


Figure 13. Plot of the asymptotic solution for $n(x, y)$ versus x and y for one period of the propagating RF wave for the solution shown in Fig. 12, where the x component of the RF electric field at the vane tips is four times that of Fig. 5. Note the structure in the foreground, which is the spoke of charge, and is now much larger. The slow oscillation seen near the cathode and deep in the sheath is again due to the 'magnetron resonance', where $\omega_e = \Omega$. However since $\omega_0 < \Omega$ still, the resonance does not occur inside the physical region, and one is only seeing a disturbance due to its close proximity in phase space.

Now let us consider a solution when the ambient magnetic field is much smaller; $\Omega = 0.833\omega_0$, and $V = 0.80$. Taking the x component of the RF electric field at the anode to be 50% larger than in Fig. 5, we have the resulting densities n_0 and $|n_1|$ as shown in Fig. 14. Using this amplitude for the RF fields and combining these values with the proper phases and adding, we obtain Fig. 15. One should note that the

https://doi.org/10.1017/S0022377897006363 Published online by Cambridge University Press

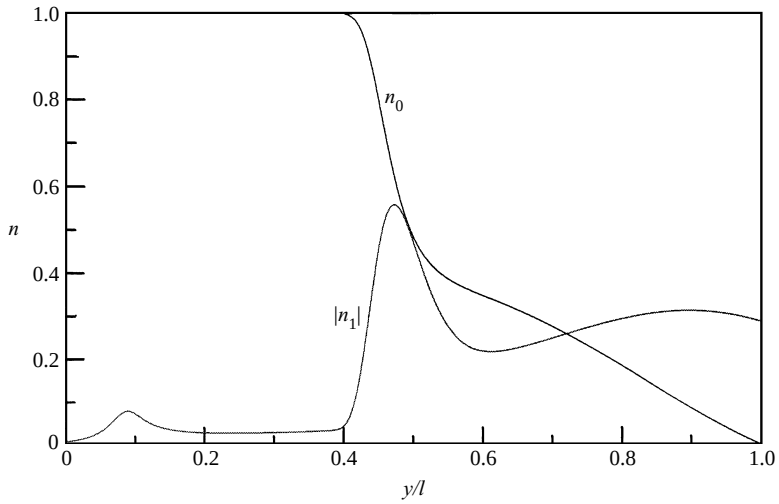


Figure 14. Plot of the magnitude of the RF density $n_1(y)$ in comparison with the background density $n_0(y)$ for a lower-magnetic-field case; $V = 0.80$ and $\Omega/\omega_0 = 0.833$. Here we can only take the RF amplitudes to be 50% larger than that in Fig. 5.

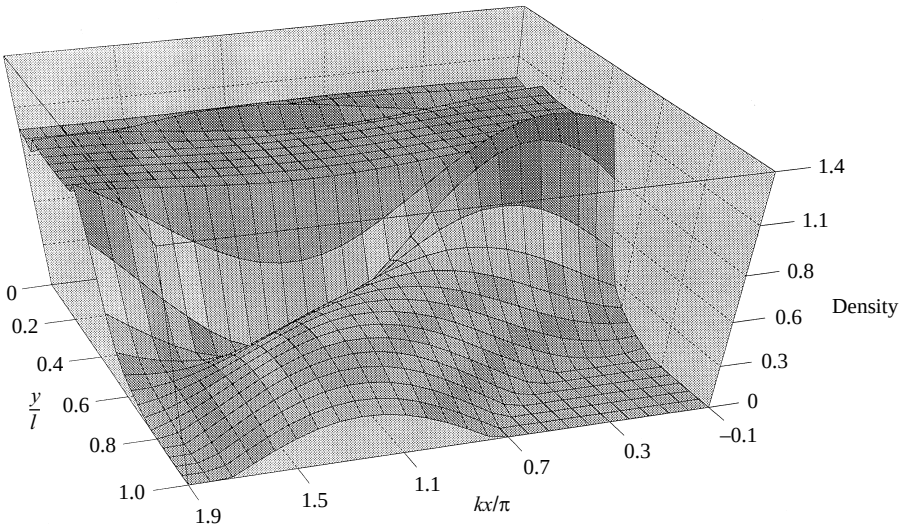


Figure 15. Plot of the asymptotic solution for $n(x, y)$ versus x and y for one period of the propagating RF wave for the solution shown in Fig. 14, where the x component of the RF electric field at the vane tips is 50% larger than that of Fig. 5. Note the structure in the foreground, which is the spoke of charge, and is still much larger. The slow oscillation now seen above the cathode but still deep in the sheath is again due to the 'magnetron resonance', where $\omega_e = \Omega$. For this case, $\omega_0 > \Omega$ and the resonance now occurs inside the physical region. However, its amplitude is much smaller than in the other two cases.

magnetron resonance (Antonsen *et al.* 1985) (where $A = 0$) now occurs inside the physical region. However, its amplitude is much smaller than before. The dominant feature is still the wave–particle resonance near $y = 0.5l$, from which the resulting spoke of charge originates, reaching up to the anode.

https://doi.org/10.1017/S0022377897006363 Published online by Cambridge University Press

4. Conclusions

We have shown that the background Brillouin flow in a CFA is significantly changed by presence of an RF wave in the slow-wave structure. Starting from a cold configuration, with the ambient magnetic field and the input RF signal present, as the DC voltage is turned on, at first one will have a Brillouin flow. However as the DC voltage is increased, one reaches a DC voltage at which the wave–particle interaction can occur between the electrons at the top of the sheath and the propagating RF wave. At this point, the Brillouin flow becomes unstable (Kaup and Thomas 1996). As a consequence of this instability, the background density profile distorts into a new shape – one that is stable and is a asymptotic, steady-state solution. Examples of these asymptotic solutions are given in Fig. 4. The DC current characteristics and the phase-shift characteristics of these solutions qualitatively agree with the known experimental characteristics of the CPI No. 266 tube. What has not been done is to determine how fast this asymptotic state will be reached inside the tube. Until this is done, we cannot make quantitative comparisons with the experimental values for the currents and phase shifts, since we do not know how much of the front of the tube is transversed before reaching these asymptotic states. This is a key problem that needs to be solved.

In spite of that, these results are very encouraging, and give us a qualitatively understanding of some of the important processes that occur inside actual devices, as well as some quantitative quantities. For example, by maximizing the amplitude of $|n_1|$ subject to $|n_1| \leqslant n_0$, except near the anode, we are able to estimate the maximum power level that can be reached, and thereby could estimate the gain from this theory.

Another problem that needs to be solved in some limit concerns the contributions of the higher harmonics to these results. We have already indicated that we should expect these to be important only near the anode, and have used this supposition to justify replacing any negative density values with zeros. So we shall give our reasons here in more detail. First, in general, the harmonics are nonresonant. For any background density profile, it could be an accident if another eigenmode could exist for any harmonic. For the first harmonic, we have $k = 2k_0$ and $\omega = 2\omega_0$, where k_0 and ω_0 are the RF wave vector and frequency of the input signal. Consequently, in general, any harmonic would be a driven solution, determined by the appropriate nonlinear source term. For the first harmonic, this source term would be proportional to the square of the RF field. Looking at Fig. 11, one notes that the RF electric fields are largest at the anode. The same is true for the RF velocities. Thus the square of either of these would extenuate this even more, causing the source terms to become significantly nonzero only near the anode. Of course, the RF density is more slowly varying, so this does not necessarily hold true for all source terms. However, when one also considers that the homogeneous solution of Poisson's equation for the first harmonic would be exponential, $\sinh(2ky)$, then these all generally indicate that the harmonic contributions, away from the anode, will generally be small. And until this could be theoretically confirmed, it seems to be a reasonable assumption to use. If it is the case then we need only appeal to the supposition that the solutions of the full cold-fluid equations will always be physical, in that the density will never go negative. Then, considering the nature of the current solutions near the anode, as in Figs 8, 13 and 15, we should expect the contributions from the harmonics to be generally destructive where the present

https://doi.org/10.1017/S0022377897006363 Published online by Cambridge University Press

densities are negative (which are shown as zero in the figures) and to be additive where these densities are positive. The net result would then be qualitatively the same as given in these figures.

We have assumed the cathode to be a perfect device and to be able to generate electrons on demand. Actual cathodes generate electrons by secondary emission. Some of this could possibly be modelled in the future by modifying our boundary condition at the cathode, which is $\partial_y \phi_0(0) = 0$. However, this is still to be explored.

One interesting feature is the existence of the magnetron instability (Antonsen *et al.* 1985), $A = 0$, deep inside the sheath. As we have seen in Figs 8 and 13 for the high-magnetic-field case, the amplitude of the variations in the particle density can be relatively large, and, since it occurs next to the cathode, it may have some important consequences for the emission properties of the cathode (Lau and Chernin 1992; Lau *et al.* 1993; Christenson and Lau 1994). One also notes that in the low magnetic-field case (Fig. 15), these oscillations are much smaller. We note that this is also the regime of ultralow noise – but whether or not these two effects are related remains to be seen.

Acknowledgements

This research has been supported in part by the Naval Surface Warfare Center, Crane Division, the ONR and the Air Force Office of Scientific Research.

References

Antonsen, T. M. Jr, Ott, E. Chang, C. L. and Drobot, A. T. 1985 *Phys. Fluids* **28**, 2878.
Brillouin, L. 1945 *Phys. Rev.* **67**, 260.
Buneman, O. Levy, R. H. and Linson, L. M. 1966 *J. Appl. Phys.* **37**, 3203.
Chan, H.-W. Chen, C. and Davidson, R. C. 1993 *J. Appl. Phys.* **73**, 7053.
Christenson, P. J. and Lau, Y. Y. 1994 *Phys. Plasmas* **1**, 3725.
Davidson, R. C. 1984 *Phys. Fluids* **27**, 1804.
Davidson, R. C. 1985 *Phys. Fluids* **28**, 1937.
Davidson, R. C. and Tang, K. T. 1985 *Phys. Fluids* **28**, 1169.
Davidson, R. C. Chan, H.-W. Chen, C. and Lund, S. 1991 *Rev. Mod. Phys.* **63**, 341.
Desjarlais, M. P. and Sudan, R. N. 1986 *Phys. Fluids* **29**, 1245.
Desjarlais, M. P. and Sudan, R. N. 1987 *Phys. Fluids* **30**, 1536.
Dombrowski, G. E. 1988 *IEEE Trans. Electron Devices* **35**, 2060.
Drazin, P. G. and Reid, W. H. 1981 *Hydrodynamic Stability*, Chap. 4. Cambridge University Press.
Jablonski, M. K. 1992 A comparison of linear perturbation analysis with computer simulation results for a planar magnetron. MIT.
Kaup, D. J. and Thomas, G. E. 1989 *Stud. Appl. Maths* **81**, 37 [Erratum **83**, 271(E) (1990].
Kaup, D. J. and Thomas, G. E. 1992 *Phys. Fluids* **B4**, 2640.
Kaup, D. J. and Thomas, G. E. 1996 *Phys. Plasmas* **3**, 771.
Kaup, D. J. and Thomas, G. E. 1997 *J. Plasma Phys.* **58**, 145.
Lau, Y. Y. and Chernin, D. *Phys. Fluids* **B4**, 3473.
Lau, Y. Y. Christenson, P. J. and Cherin, D. *Phys. Fluids* **B5**, 4486.
Palevski, A. Bekefi, G. and Drobot, A. 1981 *J. Appl. Phys.* **52**, 4938.
Prasad, S. A. Morales, G. J. and Fried, B. D. 1987 *Phys. Fluids* **30**, 3093.
Riyopoulos, S. 1993 *Phys. Rev.* **E47**, 2839.
Riyopoulos, S. 1996 *Phys. Plasmas* **3**, 1137.
Slater, J. C. 1959 *Microwave Electronics* Chap. 13. Van Nostrand, Princeton, NJ.

https://doi.org/10.1017/S0022377897006363 Published online by Cambridge University Press